Bulletin of Earthquake Engineering
https://doi.org/10.1007/s10518-025-02108-x

ORIGINAL ARTICLE

Geotechnical assessment of the 2023 Jajarkot Nepal Earthquake using field observations and remote sensing

Rajan KC[1] · Richa Pokhrel[1] · Prabin Acharya[2] · Keshab Sharma[3] · Mandip Subedi[4] · Shikshita Bhandari[5] · Kabin Lamichhane[1]

Received: 27 July 2024 / Accepted: 19 January 2025

Abstract
On November 3, 2023, at 23:47 local time, a M_W 5.7 earthquake struck Barekot in northwest Nepal at a depth of approximately 12 km. Although the region has been predicted to experience a major earthquake, this moderate-sized earthquake was the most severe seismic event in 518 years. Despite its relatively low magnitude, the earthquake caused significant damage, resulting in 154 deaths and the collapse of over 26,557 houses. This underscores the critical need for post-earthquake reconnaissance to identify vulnerabilities and improve mitigation strategies before more severe events occur. Recognizing this importance, a detailed reconnaissance was conducted from November 6 to 9, 2023, focusing on the geotechnical impact of the earthquake. Based on the field observations, this paper discusses several geotechnical issues triggered by earthquakes in the region, including shallow landslides, rockfalls, and structure damage to flexible pavement and retaining walls. The study also explores the potential triggering mechanisms for the rock fall and discusses possible remedial techniques. Additionally, the influence of the local site effect on the extent of damage was examined. Remote sensing techniques were employed to detect post-earthquake ground patterns and land use changes using Sentinel-1 and Sentinel-2 images, respectively. The Sentinel-1 images were analyzed using the persistent scattering interferometric synthetic aperture radar (PS-InSAR)-based method, and the Sentinel-2 images were analyzed via the Google Earth Engine (GEE). By assessing these geotechnical impacts, this study aims to enhance earthquake preparedness in the future and provide valuable insights for engineers and policymakers to reduce risks and improve disaster resilience.

Keywords Jajarkot earthquake · Geotechnical effects · Landslides · Topographic effect · Remote sensing · Local site effect

Extended author information available on the last page of the article

Published online: 31 January 2025

1 Introduction

A moment magnitude (M_W) 5.7 (local magnitude, M_L 6.4) earthquake struck Jajarkot district on November 3, 2023, approximately 330 km northwest of Kathmandu, the capital city of Nepal. The epicenter of the earthquake was located at Ramidanda village (N: 28°51'28.8", E: 82°9'10.8") at a focal depth of approximately 12 km (USGS 2023). Two major aftershocks, M_W 5.3 and M_W 4.0, followed the mainshock (DMG 2023). The 2023 Jajarkot Earthquake is mainly associated with interactions among the Himalayan frontal thrust (HFT), main boundary thrust (MBT), and main central thrust (MCT). The shaking intensity estimated was around VIII on the MSK scale (Fig. 1). The ground motions recorded during the mainshock at the Bhimchula station (nearest to the epicenter) indicated a peak ground acceleration (PGA) reaching up to 70 cm/s² (Subedi et al. 2024). The earthquake was of relatively low magnitude but affected Jajarjot, Rukum West, and Salyan, with a total death count of at least 154 and the complete collapse of over 26,557 residential houses (USGS 2023; KC et al. 2024a). In addition to structural failures, the cascading impacts of earthquakes were landslides, rockfalls, and damage to various road infrastructures, particularly along the national highways.

Nepal, located in the center of the Hindu Kush Himalaya, which is one of the most seismically active zones in the world (Bajracharya and Shrestha 2011; Bolch et al. 2019; Nepal et al. 2018; Putti and Satyam 2018). The country has experienced numerous earthquakes throughout its history, with major earthquakes occurring in 1255, 1408, 1505, 1681, 1810, 1866, 1934, 1980, 1988, and 2015, most of them affecting central and eastern part (Acharya et al. 2023; Chaulagain et al. 2018; Gautam and Chaulagain 2016; Prakash et al. 2016). While most of these earthquakes have primarily affected the eastern part of the country, some seismic events like the 1505 earthquake (approximately M_W 8.2), significantly impacted the western region, underscoring its vulnerability to seismic hazards (Chaulagain et al. 2015; Kumar et al. 2006; Subedi et al. 2024). However, western Nepal has not experienced a major destructive earthquake for over 500 years, leaving its seismic performance largely unknown. This long seismic gap indicates a buildup of substantial strain energy, raising the concern about the possibility of major or even mega-scale earthquake in the region (Ghazoui et al. 2019; Srivastava et al. 2015).

Geotechnical reconnaissance following an earthquake is vital for understanding the effects on infrastructure and natural landscapes, assessing hazards, and planning mitigation strategies (Cetin et al. 2021; Lanzo et al. 2019; Malakar et al. 2023; Walker et al. 2021). For example, after the 1994 Northridge earthquake in California, reconnaissance identified damage to retaining walls and slopes, leading to improved design standards for seismic resilience (Engelhardt and Sabol 1997; Sabol 2004). In Nepal, the first well-documented earthquake was 1934 Nepal-Gorkha Earthquake, which primarily focused on structural damage and fatalities. Comprehensive geotechnical assessment in Nepal was conducted only after the 2015 Gorkha Earthquake. The post-earthquake reconnaissance by Hashash et al. (2015), Sharma and Deng (2019), Chiaro et al. (2015), Gautam (2017), Okamura et al. (2015), and Konagai et al. (2015) focused on geotechnical impacts in central and eastern Nepal. The field investigations of 2015 Gorkha Earthquake revealed widespread landslides and soil liquefaction, which were essential for guiding reconstruction efforts and updating building codes. In fact, Chiaro et al. (2015) highlighted key geotechnical aspects of the 2015 Gorkha Earthquake, including ground shaking amplification on soft soils in Kathmandu,

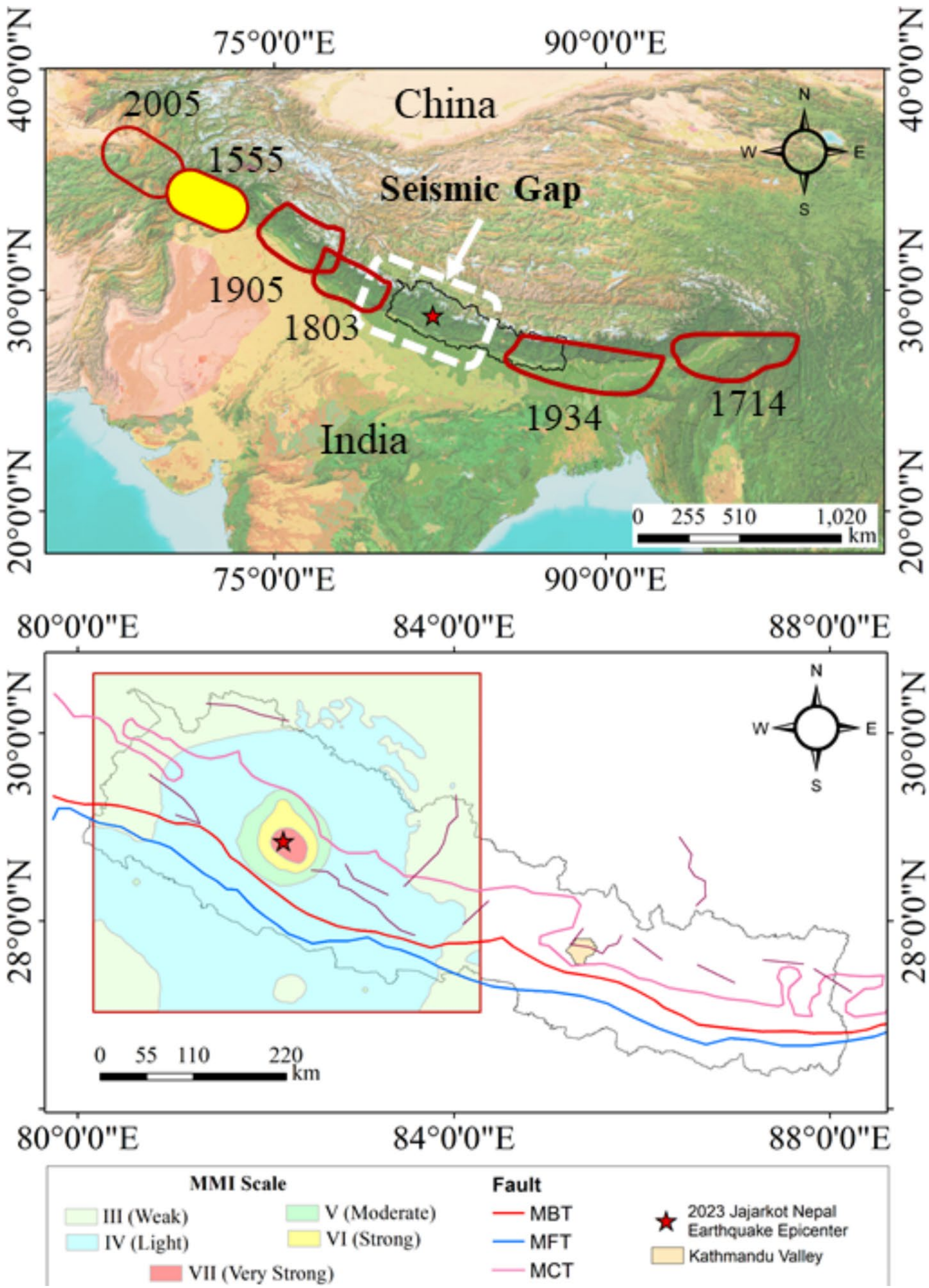

Fig. 1 Study area map of Nepal showing seismic gap in western part of the country, epicenter of the 2023 Jajarkot Earthquake, intensity distribution and faults

widespread landslides and rockfalls, evidence of liquefaction at the Trishuli dam, and the need for comprehensive site investigations and slope stability assessments to mitigate future risks.

Post-earthquake reconnaissance is also crucial for medium-sized earthquake, as it provides insights into the performance of structures and natural systems under moderate seismic stress, helping to identify vulnerabilities before more severe events occur (Sheshov et al. 2022). For example, the 2014 South Napa earthquake in California, with a magnitude of 6.0, revealed unexpected damage to modern buildings and infrastructure, leading to revisions in building codes and practices (Galloway and Ingham 2015; Johnson and Mahin 2016). By studying the impacts of medium earthquakes, engineers and policymakers can enhance design standards, improve hazard maps, and implement targeted mitigation strategies, ultimately reducing the risk and potential damage from future larger earthquakes. Understanding this importance, a field visit was conducted in the earthquake-affected area from November 6 to 9, following the 2023 Jajarkot Earthquake. The reconnaissance focused on landslides, rockfalls, pavement damage, and other geotechnical issues in the region.

In addition to field-based reconnaissance, a regional remote sensing analysis has been conducted. This analysis compares post-earthquake changes with pre-disaster baselines and can aid in quantifying the impacts of the earthquake event. To complement field findings, Sentinel-1 and Sentinel-2 images are analyzed using persistent scatterer interferometric synthetic aperture radar (PS-InSAR) and the Google Earth Engine (GEE), respectively. Vegetation indices such as the normalized difference vegetation index (NDVI) (Rouse et al. 1974) and soil-adjusted vegetation index (SAVI) (Huete 1988) were used to detect changes in land cover after earthquakes. By analyzing Sentinel-2 images before and after the earthquake, we identified significant changes and correlated them with ground deformation data from PS-InSAR, which measures surface displacement over time. The integration of traditional reconnaissance methods with advanced remote sensing techniques improves the accuracy of damage assessment and provides a comprehensive approach for studying earthquake effects (Rathje and Adams 2008; Rathje and Franke 2016).

By investigating and analyzing the geotechnical effects of seismic events, readiness for future earthquakes can be improved, ultimately saving lives and protecting infrastructures (Alberto et al. 2018; Anbazhagan et al. 2019; Ersoz et al. 2024; Ishikawa et al. 2021; Ko et al. 2023; Ziotopoulou et al. 2022). This study can serve as a reference for policymakers and engineers in Nepal as well as for other South Asian countries having similar socio-economic, tectonic, and building typology conditions.

2 Seismotectonics of the Nepal Himalaya

Approximately 50 million years ago, the Himalayan Mountains were formed as the result of a collision between the Indian and Tibetan Plates (Chamlagain and Gautam 2015). The continuous convergence of the plates governs the seismotectonic features in the Himalayas, leading to the occurrence of earthquakes in these regions. Situated at the center of the Himalaya concave chain, the Nepal Himalaya is categorized into four significant tectonic zones from south to north: the sub-Himalaya (SH), the lesser Himalaya (LH), the greater Himalaya (GH) and the Tethyan Himalaya (TH). These zones are separated by the main boundary thrust, main central thrust, and southern Tibetan detachment (Bollinger et al. 2004). The southern boundary is connected to the main frontal thrust, while the northern border is linked to the Indus-Tsangpo suture zone. GPS measurements in the Nepal region suggest 40–50 mm/year of northward convergence of the Indian continent compared to stable Eurasia, which is absorbed by a combination of crustal shortening and horizontal shearing (Hashash et al. 2015; Patriat and Achache 1984). The MFT, which is situated in the southern region, divides the sedimentary rocks of the Sub-Himalayan (Siwalik) sequence, which predominantly consists of conglomerate, mudstone, and sandstone from the Gangetic Plains known as Terai (Avouac 2003). The low-grade metamorphic rocks (such as phyllite, slate, quartzite, and schist) of Lesser Himalayan sequence and the metamorphic rocks from Siwalik sequence are separated by the MBT (Upreti 1999). Similarly, the MCT separates high-grade metamorphic rocks (such as schist, gneiss, and granite) of the Higher Himalayan sequence and those of the Lesser Himalayan sequence. Furthermore, the Higher Himalayan sequence and sedimentary sequence (comprising limestone) is divided by southern Tibetan detachment (STDS) (Chamlagain and Suwal 2010; Haneberg et al. 2022).

3 Methodology

3.1 Reconnaissance study

Following the mainshock of November 3, Jajarkot Nepal Earthquake, a team of the Nepal Geotechnical Society (NGS), visited the affected region from November 6 to 9, 2023. The post-earthquake reconnaissance involved a systematic approach, beginning with the immediate deployment of a multidisciplinary team to the affected area. Field investigations focus on assessing earthquake induced landslides, rockfall, and other geotechnical hazards through direct observation and data collection. Figure 2 illustrates route taken by the team during the reconnaissance.

3.2 Remote sensing

Sentinel-1 and Sentinel-2 satellite imageries were acquired over the study area, providing high-resolution SAR and multispectral data. The images underwent multiple preprocessing steps to ensure data accuracy and consistency. The Sentinel-2 images were analyzed using GEE, a cloud platform that enables researchers to manage extensive geo-data for various remote sensing tasks. GEE offers large-scale satellite imagery, robust computing power, a user-friendly API, and machine-learning tools (Pérez-Cutillas et al. 2023; Tamiminia et al. 2020). The analysis in the GEE involved developing code to extract spectral indices and detect changes before and after the earthquake. The spectral indices used in this study included the NDVI and SAVI. The calculation formulae for NDVI and SAVI are presented in Table 1. Spectral index maps for the three affected districts, both before and after the earthquake, were obtained. Additionally, index maps, mean indices, and changes in areas before and after the earthquake were obtained for the region where the reconnaissance study was performed.

The Sentinel-1 images (details shown in Table 2) were utilized to perform PS-InSAR analysis using the Stanford Method for Persistent Scatters (StaMPS) for Persistent Scatter Interferometry (PSI) (Hooper et al. 2018). The analysis involved data acquisition from

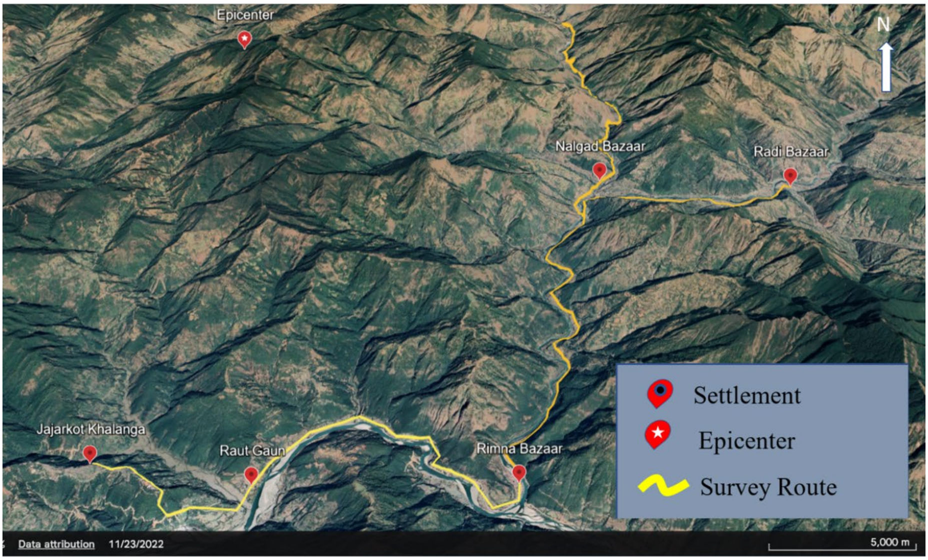

Fig. 2 Epicenter with its enlarged view and field reconnaissance route after the 2023 Jajarkot Earthquake

Table 1 Calculation details of the considered spectral indices

S.*N*.	Index	Calculation formula
1	NDVI	$=\frac{NIR-Red}{NIR+Red}=\frac{B8-B4}{B8+B4}$
2	SAVI	$=(1+L)\frac{NIR-Red}{NIR+Red+L}=(1+L)\frac{B8-B4}{B8+B4+L}$

where L is the soil brightness factor, and a value of 0.5 is used

Table 2 Details of the images considered for the PS-InSAR analysis

Product type	Sentinel-1 IW Level-1 SLC
Date	2023 March to 2024 April
Revisit period	12 days
Total images	30
Mode	Descending
Relative orbit	92
Polarization	VV
Mean incident angle	39.37°

Copernicus Open Access, data preprocessing, PSI Analysis, and data visualization. Details about the analysis process are available in Hooper et al. (2018), which has been validated in prior studies (Acharya et al. 2024).

4 Field observations

During the reconnaissance 2023 Jajarkot Earthquake, various failures were observed, including landslides, rockfall, pavement cracks, and damage to retaining walls. The geotechnical failures documented within the earthquake affected regions of Jajarkot and Rukum West are listed in Table 3 .

4.1 Landslides

Despite the relatively low magnitude of the 2023 Jajarkot Earthquake, numerous dry and shallow landslides were observed, primarily along the roadside slope. The significant number of landslides is attributed to combination of steep slopes, reaching up to 70 degrees, and presence of several-meter-deep layer of fractured and highly weathered materials in the terrain. The landslide along the Bheri corridor were mainly characterized by a mix of rock boulder, silt and sand. The observed landslides along the reconnaissance route are demonstrated in Fig. 3.

During the 2023 Jajarkot Earthquake, local authorities effectively managed road blockages caused by road side landslides. This prevented significant transportation disruptions, although rapid rescue efforts were impacted. In the mountainous terrain of Nepal, where many roads share the same origin, blockages on primary routes during an earthquake can severely disrupt transportation networks, isolating communities from rescue and relief efforts. According to (KC et al. 2023), landslide occurrences are clustered both spatially and temporally, with 93.26% of all landslides taking place during the monsoon season. Tension cracks induced by earthquakes could lead to additional landslides during the rainy season. This can lead to mass debris deposition downstream of rivers and riverbed uplift and may impact agricultural lands on riverbanks. Moreover, earthquake preconditioning can make the land more vulnerable to landslides following a seismic event and can last up to 8–10 years. After the 2015 Mw 7.8 Gorkha Earthquake in Nepal, there was a significant rise in landslide disasters, especially in the central-eastern regions (KC et al. 2024a).

Nepal's topography is relatively uniform from east to west, encompassing the flat Terai region up to 600 m in the south, hilly terrain in the middle, ranging from 800 m to 3000 m, and Higher Himalayan peaks surpassing 8000 m in the north, all of which are measured above mean sea level. The uniform topography from east to west provides a slight estimation of the performance of the western terrain following the 2015 Gorkha Earthquake. According to Collins and Jibson (2015), the total area of Nepal impacted by 2015 Gorkha Earthquake was approximately 30,000 km^2. Several landslides reached an immense volume, exceeding 250,000 m^3. This highlights Nepal's significant vulnerability to coseismic landslides.

Table 3 Location and general description of the geotechnical failure observed during the 2023 Jajarkot Earthquake

SN	Northing	Easting	Description	Fig. No
1	28°42'49.5"	82°14'47.3"	Small to medium size rock fall along with debris flow on the Bheri corridor	3a
2	28°42'14"	82°15'31"	Landslides on Bheri corridor's lower slope in Bheri river side	3b
3	28°41'54.7"	82°15'46.9"	Falling of boulder and sand mixed overhanging mass	3c
4	28°47'06.1"	82°17'33.5"	Shallow landslides on the roadside	3d
5	28°48'07"	82°17'22"	Shallow landslide along the road at Nalgad Bazaar, along the Bheri Corridor	3e
6	28°41'19.6"	82°13'53"	Landslide blocking of the Bheri Corridor	3f
7	28°42'09.9"	82°15'45.8"	Rock fall along Bheri Corridor	4a
8	28°42'49"	82°15'25"	Rockfall with maximum size upto 5.8 m^3	4b
9	28°42'29.5"	82°14'17.8	Rockfall blocking the Midhill Highway	4c
10	28°47'39.1"	82°18'14.1"	Rock fall	4d
11	28°42'29"	82°14'17"	Wedge failure	4e
12	28°42'17"	82°14'08"	Large size rock falls up to 1.73 m^3 Midhill Highway	4f
13	28°48'05"	82°17'25"	failure of roadside slope retaining wall local road nearby Nalgad Bazaar	6a
14	28°42'15"	82°14'07"	Damage to concrete barriers along Midhill Highway	6b
15	28°42'17"	82°14'08"	Rockfall that caused pot holes on the road	6c
16	28°41'57"	82°15'46.9"	Transverse crack	8a
17	28°42'21"	82°15'19"	Longitudinal crack in road	8b
18	28°42'27"	82°15'32"	Edge depression on roadside	8c
19	28°42'03"	82°16'46"	Cracking of ground surface near road edge	8d
20	28°41'54.7"	82°15'46.9"	Diagonal shear crack on flexible pavement	8e
21	28°42'03"	82°16'42"	Diagonal crack of edge nearby the Rimna Bridge (RCC)	8f

4.2 Rock fall

Figure 4 shows observed rockfalls along the reconnaissance route. Rock falls of varying sizes, ranging from 0.5 m^3 to as large as 5.8 m^3, were observed at different locations along the highway. The variation in size was caused by the falling of multiple discrete boulders at some locations and the fragmentation of large rock blocks during rolling and bouncing from greater heights at other locations. According to Marzorati et al. (2002), the Umbria-

Fig. 3 Field observations of landslides triggered by the earthquake, illustrating the range of slope instabilities observed in the affected region: **a** a debris slide obstructing a local road, **b** erosion and instability near a riverbank, highlighting geomorphic changes, **c** collapsed slopes impacting roadways and nearby vegetation, **d** large-scale slope instability near settlements, **e** a steep hillside showing clear evidence of mass movement, and **f** a road embankment destabilized by landslide debris

Marche 1997 earthquake, which had the same magnitude as the Jajarkot Earthquake (M_W 5.7), triggered significant rockfalls and landslides. Therefore, a cascading impact from this earthquake could occur, potentially triggering more rockfalls and landslides during the rainy season.

The rockfall during the 2023 Jajarkot Earthquake did not result in any recorded casualties. However, it caused significant damage to pavement and road protection structures. Damage to retaining wall was observed along the roadside slope near Nalgad Bazaar, as illustrated in Fig. 5a. The impact of rock fall destroyed the roadside concrete barrier, as shown in Fig. 5b. Additionally, it caused potholes in pavement that were up to 1.8×2.3 m (Fig. 5c). The occurrence of rockfall is influenced by the terrain and the mechanical properties of the rock. The failure mechanism of rock fall includes plane failure, wedge failure, and toppling failure.

In the hilly regions of Nepal, roads construction often involves extensive cut and fill operation (Fig. 6). This method involves excavation into the weathered bedrock on one side of the road and using that material to fill up the opposite side (KC et al. 2024b; Sharma and

Fig. 4 Examples of rockfalls triggered by the earthquake, demonstrating the direct impact on road infrastructure and slope stability: **a** rock blocks detached from steep slopes and deposited on roads, **b** large boulders blocking critical roadways, causing transportation disruptions, **c** accumulation of rock debris along roadsides, **d** evidence of fractured rock mass indicating seismic shaking effects, **e** collapsed rock slopes near inhabited areas, and **f** a displaced boulder resting on a damaged road section

Deng 2019). During reconnaissance of 2023 Jajarkot Earthquake, numerous steep cuts and slope adjacent to it failed along the road. Additionally, the outer margins of many roads either failed or exhibited extensive fissuring due to insufficient compaction of the fill material during construction.

Rock foliation and bedding planes (Fig. 4d) significantly influence the stability of cut-and-fill roads during earthquakes. These natural rock features can become potential slip surfaces, particularly when they align parallel to or slope towards the road cut. During seismic events, these planes can slip and cause rockslides or collapses, jeopardizing road safety. For instance, the 1994 Northridge earthquake led to failures of cut-and-fill slopes in foliated rock areas (Holzer et al. 1999). To design and reinforce roads effectively against earthquake risks, it is essential to understand the orientation and properties of these rock layers.

This highlights the high vulnerability of the roads to rockfall and underscores the need for effective protective measures to enhance road safety and stability. Flexible geosynthetics, as shown in Fig. 7a, can be deployed in areas prone to frequent rock falls. A flexible net absorbs the impact of falling rocks and creates a platform for their collection. This mecha-

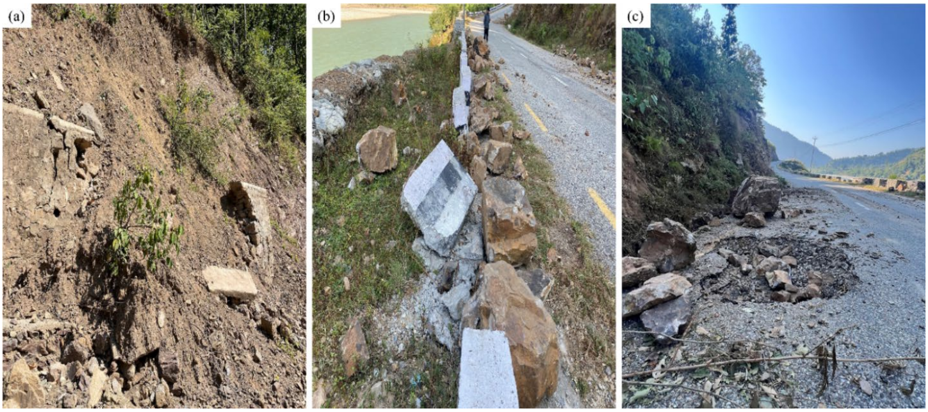

Fig. 5 Damages caused by landslides and rockfalls to road infrastructure and protective measures: **a** slope instability leading to debris accumulation along a highway and failure of an unreinforced masonry retaining wall, **b** damage to a concrete barrier, and **c** crater-like damage on a road surface caused by falling boulders

Fig. 6 **a** Typical road construction in hilly terrain consisting of cut and fill, **b** schematic diagram of the rock fall along the highway section

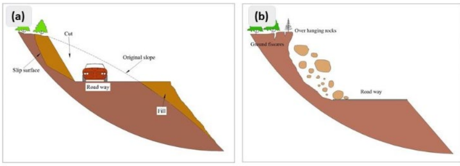

nism is also utilized in reinforced gabions (Fig. 7b). Additionally, ditches alongside roads can serve as another solution, with the width of the ditch varying based on the slope of the terrain (Fig. 7c). Steeper slopes, where rocks fall directly into ditches, necessitate a narrower width, while gentler terrains, where rocks may roll or bounce, require a wider width.

4.3 Pavement failure

During reconnaissance, both lateral and longitudinal cracks were observed on the existing flexible pavement. Lateral cracking was observed across the entire cross-section, and longitudinal cracking extended up to 120 m along the road surface. The details of such failures are depicted in Fig. 8a and b. Lateral cracking of this type is caused by horizontal movement on the earth's surface, leading to fractures perpendicular to the road surface. Both the shearing force and horizontal movement during an earthquake contribute to longitudinal cracking. Figure 8c and d show the fissures and depressions on the road edge adjacent to the China Bazaar. Figure 8c depicts pavement crack with width of 0.45 m and a depth of 1.82 m. Figure 8e and f depict a diagonal fissure close to the Rimna Bridge, highlighting

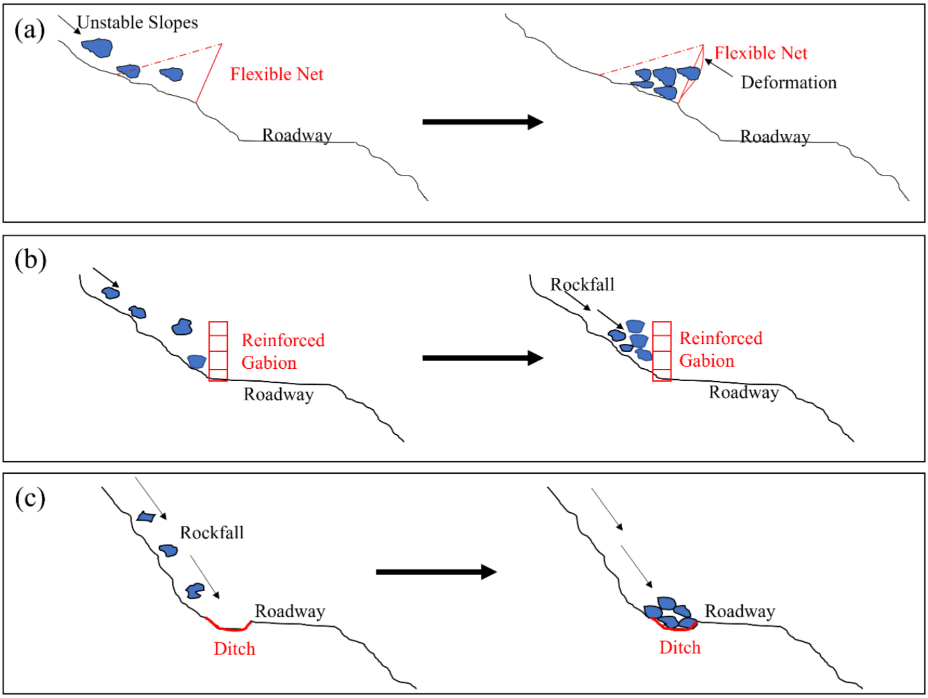

Fig. 7 Protection measures against rock fall: **a** flexible net, **b** reinforced gabion, and **c** ditches all on roadside slopes.
(modified from Jiang et al. (2021))

the interaction of compressive and shear forces during the ground displacement caused by the earthquake.

5 Local site effects

5.1 Ridge effect

Ridge effects describe the intensification of ground shaking at elevated topographic features like hills, ridges, and cliffs, caused by the focusing of seismic energy. These effects can significantly influence the intensity, frequency, and duration of shaking compared to flat terrain (Meunier et al. 2008; Sánchez-Sesma et al. 1985). Likewise, Sharma et al. (2017) mentioned that the ridge effect occurs when seismic waves interact with topographic features like ridges and hills. These waves are scattered, diffracted, and reflected upon encountering such elevated structures, creating constructive interference that amplifies ground motion. At ridge crests, seismic waves become focused and trapped, intensifying shaking. Evidence of ridge effects was observed in the stark contrast between the damage to buildings located on hills and those in adjacent valleys (Sharma and Deng 2019). Likewise, the ridge effect during the Jajarkot Earthquake is demonstrated through a distinctive pattern of damage, with a pronounced concentration at the summits of hills. Greater infrastructural damage was

Fig. 8 **a** Earthquake-induced transverse crack, **b** longitudinal crack, **c** edge depression, **d** ground fissure, **d** diagonal shear crack in pavement, and **f** diagonal shear crack near bridge

concentrated in the Jajarkot Khalanga, indicating the occurrence of topographic amplification. In contrast, Kale Gaun, which lies on relatively lower land, suffered minimal damage during the seismic event, as demonstrated in Fig. 9. The ridge effect was also observed in the Barkot and Limsa areas, where the location experienced substantial structural damage. Satyam and Towhata (2016), Satyam and Rao (2008), and Putti and Satyam (2020) highlight that local soil conditions significantly influence seismic risk, as evident during the Jajarkot Earthquake.

During the 2015 Gorkha Earthquake, ridge effect was seen in the Kathmandu Valley. structures at the top of Swayambhu Nath (1426 m MASL) experienced significant damage, while building in the surrounding lowlands remained largely undamaged (Sharma and Deng 2019). Similarly, in the Sindhupalchowk district, a school situated at the top was entirely destroyed, whereas a school in the lower valley remained operational (Sharma and Deng 2019).

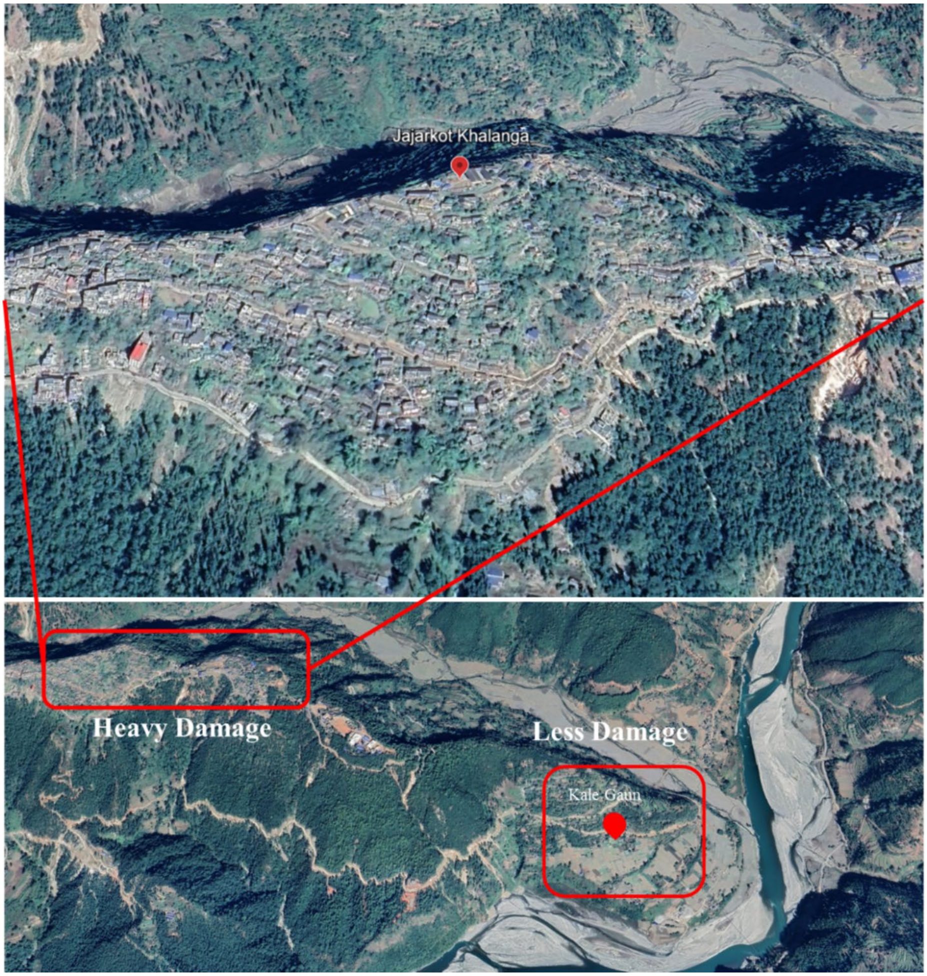

Fig. 9 Evidence of ridge effects: heavy damage in the Jajarkot Khalanga area less damage in the Kale Gaun area

5.2 Basin effects

The basin effect occurs when seismic waves enter sediment-filled basins with softer materials, where they become trapped and amplified due to the stark contrast in stiffness and density between the sediments and the bedrock. The shape of the basin also contributes to the amplification, with resonance and the generation of surface waves extending and intensifying the shaking (Sharma et al. 2016). Evidence of the basin effect was observed at Rimna Bazar, Jajarkot (1759 m MASL), where the building suffered from substantial damage, as shown in Fig. 10a. This effect was also observed in Raut Gaun, Jajarkot (802 m MASL), as shown in Fig. 10b. Similar effect was evident in the Kathmandu basin during the Gorkha Earthquake. This effect was prominently seen during the 1985 Mexico City Earthquake, where the soft sediments in the basin amplified the shaking, leading to widespread

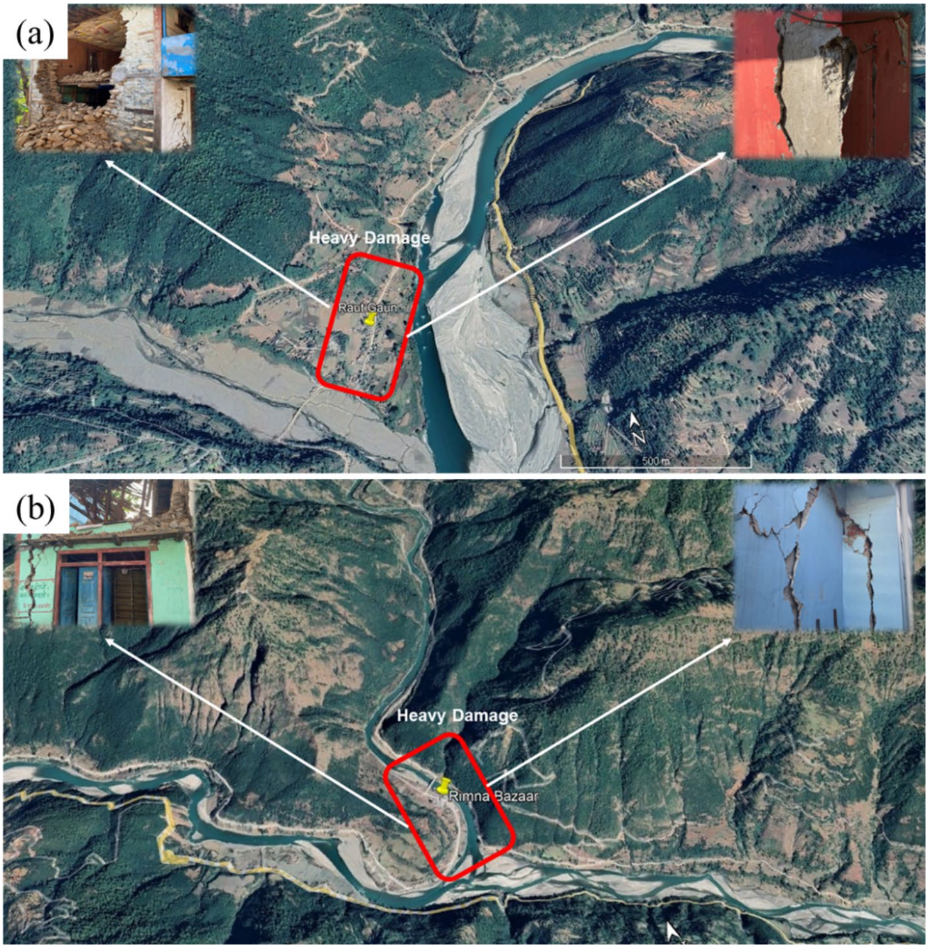

Fig. 10 Evidence of the Basin Effect in the **a** Rimna Bazaar, Jajarkot and **b** Raut Gaun, Jajarkot

destruction. Similarly, in the 2015 Gorkha Earthquake, the Kathmandu Valley experienced significant basin effects, with its thick lacustrine sediments trapping seismic waves, resulting in prolonged shaking and extensive structural damage (Abraham et al. 2015; Sharma and Deng 2019). The Kathmandu Valley basin's low-frequency amplification caused severe damage to tall, well-designed buildings, while older, low-rise masonry houses remained largely intact. This suggests that long-period ground motions amplified by soft valley sediments disproportionately affected tall buildings with long predominant periods (Hashash et al. 2015; Sharma and Deng 2019).

5.3 Soft soil effect

The soft soil effect occurs due to the low shear wave velocity, high energy dissipation, and impedance contrast between soft sediments and the underlying stiffer materials. Seismic waves slow down when traveling through these soft layers but increase in amplitude to maintain energy conservation, thereby amplifying ground shaking. This effect is intensified by the nonlinear response of soft soils during strong shaking, which alters waveforms and amplifies certain frequencies (Civelekler et al. 2021). During the 1995 Kobe Earthquake, regions with thick alluvial deposits experienced severe damage due to this effect. Likewise, in the 2015 Gorkha Earthquake, the soft sediments in the Kathmandu Valley amplified seismic waves, exacerbating the impact on historic and densely populated areas. These effects underscore the importance of understanding local site conditions in seismic hazard evaluations and the need to design resilient infrastructure in earthquake-prone areas. Similarly, this effect was evident during Jajarkot earthquake, particularly around the Bheri River, as demonstrated in Fig. 11a. For example, Fig. 11b illustrates a case where complete collapse of masonry on one side collapsed completely, while similar structure on the opposite relatively minor damage. This contract suggests the variation in the bedrock and difference in

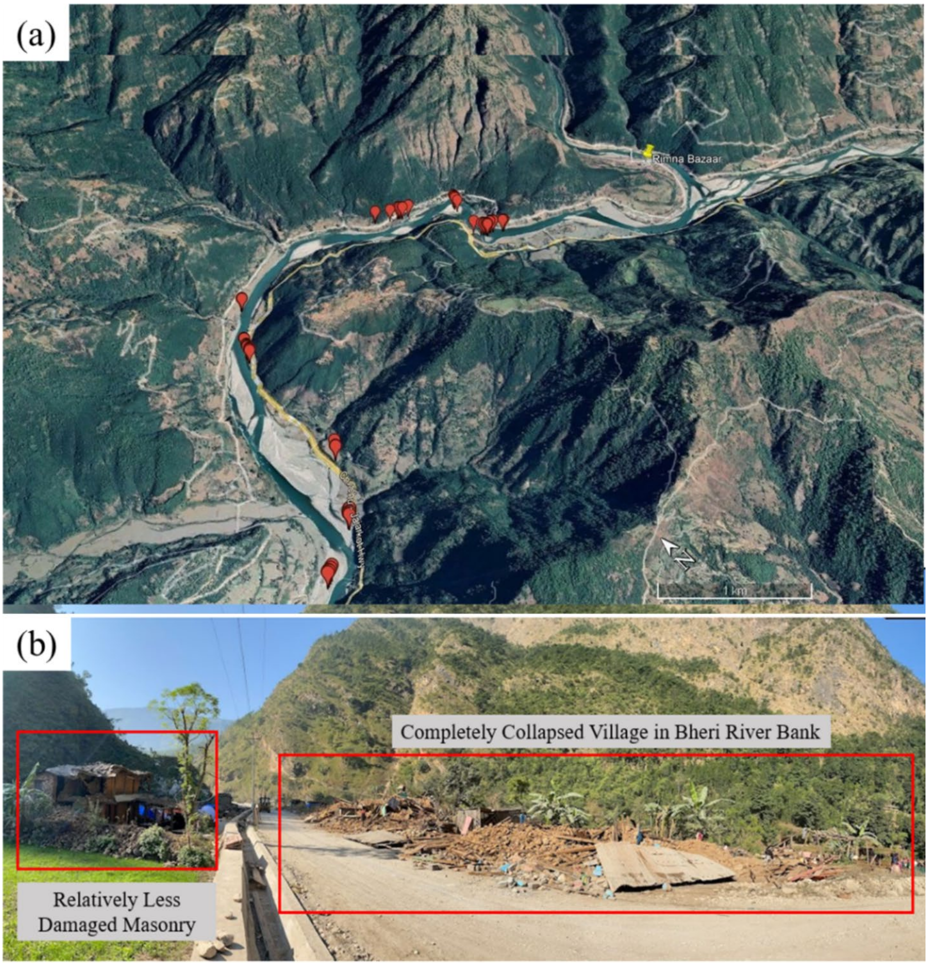

Fig. 11 **a** Locations of local site effects along the Bheri River area due to the earthquake, **b** Completely collapsed village on the river bank side and partially damaged masonry of the same kind on the opposite side representing variable ground shaking

ground shaking intensity in two sides of the road. The areas with sand and sediment deposits suffered more damage and experienced extensive failure than other locations. Similarly, extensive building damage was concentrated in the alluvial deposits of Kahramanmaras during the Turkey earthquake, demonstrating the soft soil effect (Tobita et al. 2024).

6 Remote sensing analysis

6.1 Spectral indices

NDVI and SAVI maps for the three affected districts -Jajarkot, Salyan, and Rukum West were generated using Sentinel-2 images for both the pre- and post-earthquake periods (Fig. 12). A summary of the mean values of these indices before and after the earthquake is

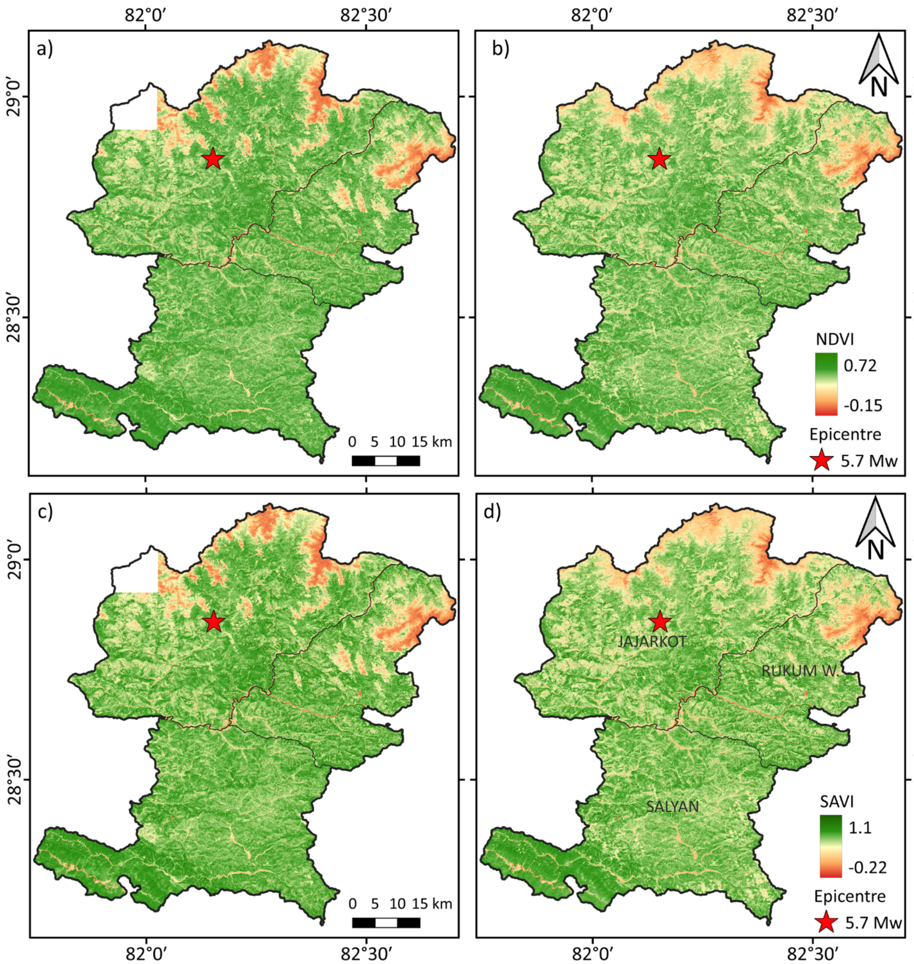

Fig. 12 The NDVI in three affected districts **a** pre-earthquake, **b** post-earthquake and SAVI, **c** pre-earthquake and **d** post-earthquake

Table 4 Changes in the NDVI and SAVI before and after the earthquake in the three affected districts (Jajarkot, Salyan, and Rukum West)

District	Mean NDVI		Mean SAVI	
	Pre-earthquake	Post-earthquake	Pre-earthquake	Post-earthquake
Jajarkot	0.4	0.35	0.6	0.53
Salyan	0.43	0.41	0.64	0.62
Rukum West	0.37	0.36	0.56	0.55

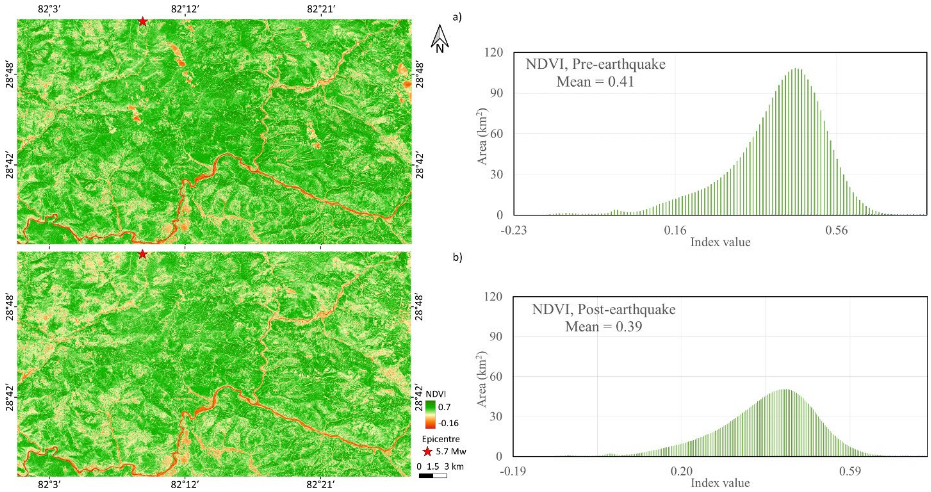

Fig. 13 The NDVI in field reconnaissance areas **a** pre-earthquake and **b** post-earthquake

Table 5 Land use types according to the change in the NDVI before and after the earthquake in the three affected districts (Jajarkot, Salyan, and Rukum West)

NDVI range*	Pre-earthquake area (km^2)	Post-earthquake area (km^2)	Land cover types
< 0	21.04	16.61	Clouds, rocks, water, concrete, asphalt
0 to 0.2	171.92	185.40	Open or bare soil
0.2 to 0.5	2394.47	2516.64	Sparse vegetation
> 0.5	624.76	493.53	Dense vegetation
Total area (km^2)	3212.19	3212.19	

*NDVI range from USGS (2024) and Sentinel Hub (2024)

presented in Table 4 . The results indicate that the earthquake's impact was most significant in Jajarkot, as evidenced by a substantial reduction in the post-earthquake NDVI and SAVI indices. In contrast, Rukum West and Salyan showed only slight reductions in these indices, suggesting a lesser impact in these districts compared to Jajarkot.

The reconnaissance area, which experienced a major impact from the earthquake, was further analyzed. The postdisaster NDVI maps, histograms, and changes in land patterns are presented in Fig. 13; Table 5. The results indicate that the open soil area increased by

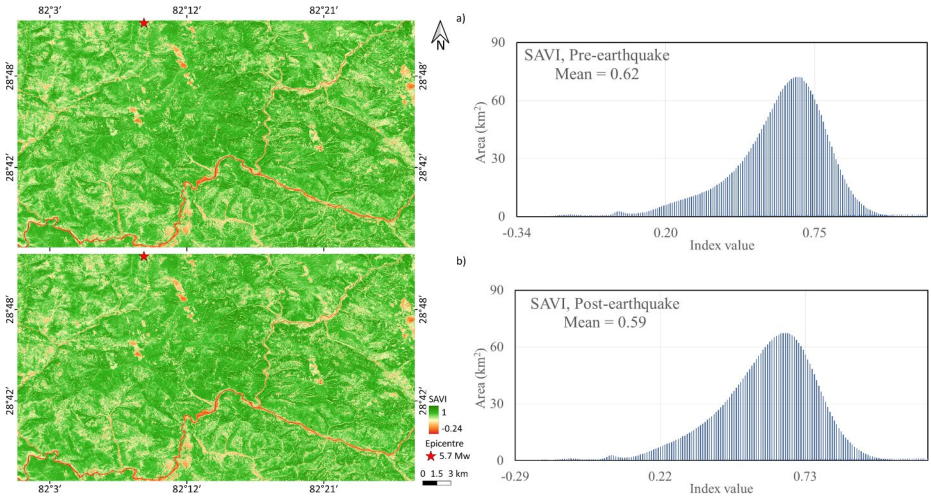

Fig. 14 The SAVI in field reconnaissance areas **a** pre-earthquake and **b** post-earthquake

Table 6 Land use types according to the change in the SAVI before and after the earthquake

SAVI range*	Pre-earthquake area (km^2)	Post-earthquake area (km^2)	Land cover types
<0	20.44	16.76	Clouds, rocks, water, concrete, asphalt
0 to 0.3	172.57	185.31	Open or bare soil
0.3 to 0.75	2365.59	2528.84	Sparse vegetation
>0.75	653.60	481.28	Dense vegetation
Total area (km^2)	3212.19	3212.19	

*SAVI range from USGS (2024) and Sentinel Hub (2024)

approximately 14.5 square kilometers after the earthquake. Similarly, the dense vegetation area decreased by approximately 130 square kilometers, transitioning to sparse vegetation.

Similarly, the SAVI maps, histograms, and variations in land patterns after the earthquake are presented (Fig. 14; Table 6). The SAVI results align with the NDVI findings, showing that open or bare soil areas increased by approximately 12.5 square kilometers after the earthquake. Additionally, there was a decrease in green areas and an increase in sparse vegetation areas of approximately 160 square kilometers, indicating that the regions were affected by the earthquake. The combined NDVI and SAVI results revealed that approximately 5% of the total area analyzed was impacted by the earthquake. These findings are consistent with observations from post-earthquake reconnaissance, which documented land cover changes such as damaged structures, as well as minor to major landslides and rockfall events. However, the pixel resolution of Sentinel imagery (10 m × 10 m) constrained the validation of individual landslide and rockfall events identified during the reconnaissance studies.

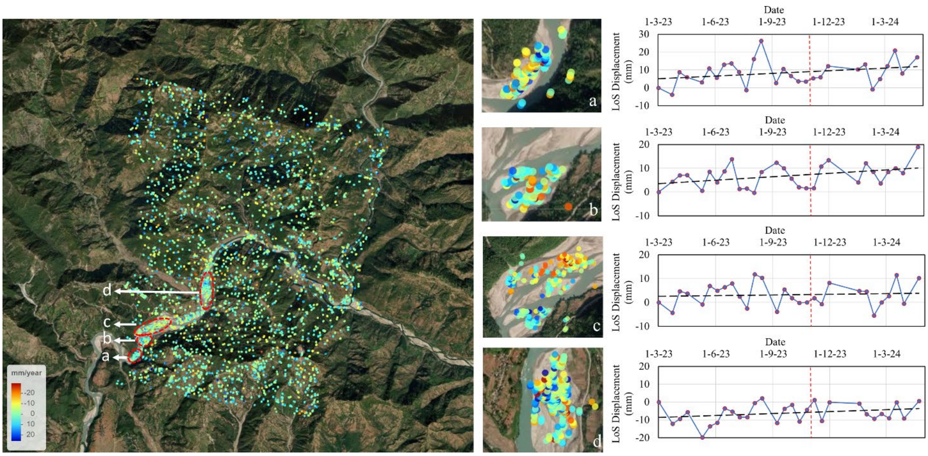

Fig. 15 The PS-InSAR line-of-sight (LoS) displacements from March 2023 to April 2024 near the reconnaissance locations with four spots further analyzed

6.2 PS-InSAR

The PS-InSAR results, showing line-of-sight displacement, are presented in Fig. 15, indicating a movement of ±20 mm. Four specific locations on the river or riverbank were further analyzed to obtain the variation in the average line-of-sight displacement over time. Overall, the PS-InSAR analysis indicated that the effects of the earthquake were localized, with no significant regional impact. There is no particular area with substantial displacement variation, suggesting an absence of major deep landslide zones, consistent with field reconnaissance results. However, the analyzed areas on the river bank show a considerable upward trend post-earthquake, with an average line-of-sight displacement of approximately 10–20 mm. This indicates increased deposition in or near the rivers following the earthquake. The increase in riverbed or riverbank levels might be attributed to the increase in bare spots and the decrease in dense vegetation areas, as indicated by changes in the NDVI and SAVI. The monsoon season may further elevate these levels, potentially triggering debris flows as well as flooding and in nearby locations.

7 Conclusions and lessons learned

This paper provides an overview of the geotechnical damage caused by the 2023 Jajarkot Nepal Earthquake observed during the reconnaissance. Despite the moderate magnitude of the earthquake, extensive landslide and rockfalls were observed. This underscores that Nepal is highly prone to coseismic landslides, making their assessment crucial for effective seismic mitigation. The observation revealed shallow landslides were particularly prevalent along the steep and weathered Bheri Corridor. The rockfalls had a significant impact on roadways, leading to failure of retaining walls and roadside barriers, as well as the formation of potholes in the pavement. Infrastructure damage was concentrated in ridges, basins, and soft soil demonstrating the local site effect during the earthquake. In addition to field reconnaissance, remote sensing analysis using NDVI and SAVI maps revealed varying degrees of earthquake impact across three districts. Jajarkot showed the most severe reduction in vegetation indices, indicating extensive damage, while Rukum West and Salyan experienced comparatively milder effects. PS-InSAR analysis indicated localized earthquake effects without widespread regional impact. Although overall displacement was limited, noticeable upward movements indicating increase in sediment deposit along riverbanks were observed post-earthquake.

The study suggests that there is a critical need for protective measures on road slopes to mitigate impacts of landslides and rockfalls even during relatively weaker earthquakes. Implementing solutions such as flexible nets, reinforced gabions, or ditches is essential to safeguard road infrastructure from frequent rockfalls. Understanding local site effects and implementing the knowledge during structural design can enhance the resilience and safety of buildings, bridges, and other vital infrastructure. However, more sophisticated studies for understanding the subsurface features of the areas should be conducted. While this study is good for planning, it is not sufficient for the detail design purpose. Comprehensive studies in other parts of the Himalayan belt are crucial for having a generalized idea of earthquake related risks and developing strategies for minimizing these risks.

The geotechnical earthquake researchers and practitioners can learn the following lessons based from this earthquake:

- The combination of steep slopes and a humid climate has led to the weathering of several meters of terrain, rendering it highly susceptible to sliding.
- The occurrence of significant landslides during this relatively weaker earthquake underscores the need for protection measures for road slopes.
- The frequent occurrence of rockfalls, along with their resulting blockage and damage to pavements, highlights the necessity for protection measures against rockfall hazards. Solutions such as flexible nets, reinforced gabions, or ditches should be considered.
- It is crucial to identify areas vulnerable to landslides and unstable rock formations in earthquake-affected areas to mitigate potential heavy damage to both humans and infrastructure during the upcoming monsoon season.
- Understanding local site effects is crucial in earthquake engineering and structural design. Engineers need to consider these variations when designing buildings, bridges, and other infrastructure to ensure their resilience and safety in the event of an earthquake.

Author contributions Rajan KC: Writing– original draft, Visualization, Validation, Methodology, Formal analysis, Data curation, Conceptualization. Richa Pokhrel: Writing– original draft, Visualization, Methodology. Prabin Acharya: Writing– original draft, Visualization, Software, Conceptualization. Keshab Sharma: Conceptualization, Validation, Writing–review & editing, Supervision. Mandip Subedi: Conceptualization, Resources, Writing– review & editing. Shikshita Bhandari: Formal analysis, Writing– review & editing, Validation. Kabin Lamichhane: Writing– original draft, Software.

Declarations

Competing interest The authors declare that they have no known competing financial interests or personal relationships that could have appeared to influence the work reported in this paper.

References

Abraham JR, Lai CG, Papageorgiou A (2015) Basin-effects observed during the 2012 Emilia earthquake sequence in Northern Italy. Soil Dyn Earthq Eng 78:230–242

Acharya IP, Subedi M, KC R (2023) Liquefaction hazard assessment of kathmandu valley using deterministic and probabilistic approaches. In: Proceedings of the Geo-Risk 2023, Arlington, VA, USA, 23–26 July 2023; ASCE, pp 307–317. https://doi.org/10.1061/9780784484968.032

Acharya P, Beier N, Liu F (2024) Cloud-based geotechnical monitoring for tailings storage facilities using sentinel remote sensing images. GeoMontreal 2024, Montreal, QC, Canada

Alberto Y, Otsubo M, Kyokawa H, Kiyota T, Towhata I (2018) Reconnaissance of the 2017 Puebla, Mexico earthquake. Soils Found 58(5):1073–1092. https://doi.org/10.1016/j.sandf.2018.06.007

Anbazhagan P, Mog K, Rao KSN et al (2019) Reconnaissance report on geotechnical effects and structural damage caused by the 3 January 2017 Tripura earthquake, India. Nat Hazards 98:425–450. https://doi.org/10.1007/s11069-019-03699-w

Avouac J-P (2003) Mountain building, erosion, and the seismic cycle in the Nepal Himalaya. Adv Geophys 46:1–80

Bajracharya SR, Shrestha BR (2011) The status of glaciers in the Hindu Kush-Himalayan region. International Centre for Integrated Mountain Development (ICIMOD)

Bolch T, Shea JM, Liu S, Azam FM, Gao Y, Gruber S, Immerzeel WW, Kulkarni A, Li H, Tahir AA (2019) Status and change of the cryosphere in the extended Hindu Kush Himalaya region. Hindu Kush Himalaya Assessment: Mountains Clim Change Sustain People. pp 209–255

Bollinger L, Avouac JP, Cattin R, Pandey MR (2004) Stress buildup in the Himalaya. J Geophys Res: Solid Earth 109:B11

Cetin KO, Cakir E, Ilgac M et al (2021) Geotechnical aspects of reconnaissance findings after 2020 January 24th, M6.8 sivrice–Elazig–Turkey earthquake. Bull Earthq Eng 19:3415–3459. https://doi.org/10.1007/s10518-021-01112-1

Chamlagain D, Gautam D (2015) Seismic hazard in the himalayan intermontane basins: an example from Kathmandu Valley, Nepal. Mountain Hazards Disaster Risk Reduct. pp 73–103

Chamlagain D, Suwal S (2010) An overview of landslide hazard in Nepal Himalaya

Chaulagain H, Rodrigues H, Silva V, Spacone E, Varum H (2015) Seismic risk assessment and hazard mapping in Nepal. Nat Hazards 78:583–602

Chaulagain H, Gautam D, Rodrigues H (2018) Revisiting major historical earthquakes in Nepal: overview of 1833, 1934, 1980, 1988, 2011, and 2015 seismic events. Impacts Insights Gorkha Earthq, 1–17

Chiaro G, Kiyota T, Pokhrel RM, Goda K, Katagiri T, Sharma K (2015) Reconnaissance report on geotechnical and structural damage caused by the 2015 Gorkha Earthquake, Nepal. Soils Found 55(5):1030–1043

Civelekler E, Okur VD, Afacan KB (2021) A study of the local site effects on the ground response for the city of Eskişehir, Turkey. Bull Eng Geol Environ 80(7):5589–5607

Collins BD, Jibson RW (2015) Assessment of existing and potential landslide hazards resulting from the April 25, 2015 Gorkha, Nepal earthquake sequence. US Geological Survey

DMG (2023) Jajarkot earthquake updates (NEMRC/SC, DMG). *Department of Mines and Geology*

Engelhardt MD, Sabol TA (1997) Seismic-resistant steel moment connections: developments since the 1994 Northridge earthquake. Prog Struct Mat Eng 1(1):68–77

Ersoz AB, Pekcan O, Altun M et al (2024) Utilizing digital technologies for rapid damage assessment and reconnaissance: the February 6, 2023 Kahramanmaraş-Türkiye earthquakes (Mw 7.7 and Mw 7.6). Bull Earthq Eng. https://doi.org/10.1007/s10518-024-01925-w

Galloway B, Ingham J (2015) The 2014 South Napa earthquake and its relevance for New Zealand. SESOC J 28(1):69–94

Gautam D (2017) Unearthed lessons of 25 April 2015 Gorkha earthquake (MW 7.8): geotechnical earthquake engineering perspectives. Geomatics Nat Hazards Risk 8(2):1358–1382

Gautam D, Chaulagain H (2016) Structural performance and associated lessons to be learned from world earthquakes in Nepal after 25 April 2015 (MW 7.8) Gorkha earthquake. Eng Fail Anal 68:222–243

Ghazoui Z, Bertrand S, Vanneste K, Yokoyama Y, Nomade J, Gajurel AP, van der Beek PA (2019) Potentially large post-1505 AD earthquakes in western Nepal revealed by a lake sediment record. Nat Commun 10(1):2258

Haneberg WC, Johnson SE, Gurung N (2022) Response of the Laprak, Nepal, landslide to the 2015 mw 7.8 Gorkha earthquake. Nat Hazards 111:567–584. https://doi.org/10.1007/s11069-021-05067-z

Hashash Y, Tiwari B, Moss RES, Asimaki D, Clahan KB, Kieffer DS, Dreger DS, Macdonald A, Madugo CM, Mason HB (2015) Geotechnical field reconnaissance: Gorkha (Nepal) earthquake of April 25, 2015 and related shaking sequence. *Geotechnical Extreme Event Reconnaisance GEER Association Report No. GEER-040*, 1

Holzer TL, Bennett MJ, Ponti DJ, Tinsley III, J. C (1999) Liquefaction and soil failure during 1994 Northridge earthquake. J Geotech GeoEnviron Eng 125(6):438–452

Hooper A, Bekaert D, Hussain E, Spaans K (2018) StaMPS/MTI manual: Version 4.1 b. *School of Earth and Environment, University of Leeds. Retrieved October*, *15*, 2019

Huete AR (1988) A soil-adjusted vegetation index (SAVI). Remote Sens Environ 25(3):295–309

Ishikawa T, Yoshimi M, Isobe K, Yokohama S (2021) Reconnaissance report on geotechnical damage caused by 2018 Hokkaido Eastern Iburi earthquake with JMA seismic intensity 7. Soils Found 61(4):1151–1171. https://doi.org/10.1016/j.sandf.2021.06.006

Jiang G, Feng Z, Zhao R, Wang F, Yu X, Wu M, Zhang Z (2021) Case study on safety assessment of rockfall and splash stone protective structures for secondary excavation of highway slope. Adv Civil Eng 1863845:9. https://doi.org/10.1155/2021/1863845

Johnson LA, Mahin SA (2016) The Mw 6.0 South Napa Earthquake of August 24, 2014. *Pacific Earthquake Engineering Research Center, Sacramento, CA*, 23–25

KC R, Sharma K, Dahal BK, Aryal M, Subedi M (2023) Study of the spatial distribution and the temporal trend of landslide disasters that occurred in the Nepal Himalayas from 2011 to 2020. Environ Earth Sci 83(1):42. https://doi.org/10.1007/s12665-023-11347-7

KC R, Lamichhane K, Sharma K, Subedi M, Bhandari S (2024a) Seismic performance of buildings during the 3rd November 2023 Jajarkot, Nepal earthquake. J Perform Constr Facil. https://doi.org/10.1061/JPCFEV/CFENG-4902

KC R, Aryal M, Sharma K et al (2024b) Development of a framework for the prediction of slope stability using machine learning paradigms. Nat Hazards. https://doi.org/10.1007/s11069-024-06819-3

Ko YY, Tsai CC, Hwang JH et al (2023) Failure of engineering structures and associated geotechnical problems during the 2022 ML 6.8 Chihshang earthquake, Taiwan. Nat Hazards 118:55–94. https://doi.org/10.1007/s11069-023-05993-0

Konagai K, Pokhrel RM, Matsubara H, Shiga M (2015) Geotechnical aspect of the damage caused by the April 25th, 2015 Gorkha earthquake of Nepal. JSCE J Disaster FactSheets

Kumar S, Wesnousky SG, Rockwell TK, Briggs RW, Thakur VC, Jayangondaperumal R (2006) Paleoseismic evidence of great surface rupture earthquakes along the Indian Himalaya. J Geophys Research: Solid Earth 111:B3

Lanzo G, Tommasi P, Ausilio E et al (2019) Reconnaissance of geotechnical aspects of the 2016 Central Italy earthquakes. Bull Earthq Eng 17:5495–5532. https://doi.org/10.1007/s10518-018-0350-8

Malakar S, Rai AK, Gupta AK (2023) Earthquake risk mapping in the Himalayas by integrated analytical hierarchy process, entropy with neural network. Nat Hazards 116:951–975. https://doi.org/10.1007/s11069-022-05706-z

Marzorati S, Luzi L, De Amicis M (2002) Rock falls induced by earthquakes: a statistical approach. Soil Dyn Earthq Eng 22(7):565–577

Meunier P, Hovius N, Haines JA (2008) Topographic site effects and the location of earthquake induced landslides. Earth Planet Sci Lett 275(3):221–232. https://doi.org/10.1016/j.epsl.2008.07.020

Nepal S, Pandey A, Shrestha AB, Mukherji A (2018) Revisiting key questions regarding upstream-downstream linkages of land and water management in the Hindu Kush Himalaya (HKH) Region. Himalayan Adaptation, Water and Resilience Research

Okamura M, Bhandary NP, Mori S, Marasini N, Hazarika H (2015) Report on a reconnaissance survey of damage in Kathmandu caused by the 2015 Gorkha Nepal earthquake. Soils Found 55(5):1015–1029

Patriat P, Achache J (1984) India–Eurasia collision chronology has implications for crustal shortening and driving mechanism of plates. Nature 311(5987):615–621

Pérez-Cutillas P, Pérez-Navarro A, Conesa-García C, Zema DA, Amado-Álvarez JP (2023) What is going on within Google earth engine? A systematic review and meta-analysis. Remote Sens Appl: Soc Environ 29:100907

Prakash R, Singh RK, Srivastava HN (2016) Nepal earthquake 25 April 2015: source parameters, precursory pattern and hazard assessment. Geomatics Nat Hazards Risk 7(6):1769–1784

Putti SP, Satyam N (2018) Ground response analysis and liquefaction hazard assessment for Vishakhapatnam city. Innov Infrastruct Solut 3:1–14. https://doi.org/10.1007/s41062-017-0113-4

Putti SP, Satyam N (2020) Evaluation of site effects using HVSR microtremor measurements in Vishakhapatnam (India). Earth Syst Environ 4:439–454. https://doi.org/10.1007/s41748-020-00158-6

Rathje EM, Adams BJ (2008) The role of remote sensing in earthquake science and engineering: opportunities and challenges. Earthq Spectra 24(2):471–492

Rathje EM, Franke K (2016) Remote sensing for geotechnical earthquake reconnaissance. Soil Dyn Earthq Eng 91:304–316

Rouse JW, Haas RH, Schell JA, Deering DW, Harlan JC (1974) Monitoring the vernal advancement and retrogradation of natural vegetation. NASA/GSFC, Type III, Final Report. https://ntrs.nasa.gov/citations/19740022614

Sabol TA (2004) An assessment of seismic design practice of steel structures in the United States since the Northridge earthquake. Struct Des Tall Special Build 13(5):409–423

Sánchez-Sesma FJ, Bravo MA, Herrera I (1985) Surface motion of topographical irregularities for incident P, SV, and Rayleigh waves. Bull Seismol Soc Am 75(1):263–269

Satyam DN, Rao KS (2008) Seismic site characterization in Delhi region using multi channel analysis of shear wave velocity (MASW) testing. Electron J Geotech Eng 13:167–183

Satyam ND, Towhata I (2016) Site-specific ground response analysis and liquefaction assessment of Vijayawada city (India). Nat Hazards 81:705–724. https://doi.org/10.1007/s11069-016-2166-7

Sentinel Hub (2024) Data retrieved from: https://custom-scripts.sentinel-hub.com/custom-scripts/sentinel-2/ndvi/ and https://custom-scripts.sentinel-hub.com/custom-scripts/sentinel-2/savi/

Sharma K, Deng L (2019) Reconnaissance report on geotechnical engineering aspect of the 2015 Gorkha, Nepal, earthquake. J Earthq Eng 23(3):512–537

Sharma K, Deng L, Noguez CC (2016) Field investigation on the performance of building structures during the April 25, 2015, Gorkha earthquake in Nepal. Eng Struct 121:61–74

Sharma K, Subedi M, Parajuli RR, Pokharel B (2017) Effects of surface geology and topography on the damage severity during the 2015 Nepal Gorkha earthquake. Lowland Technol Int 18(4):269–282

Sheshov V, Apostolska R, Bozinovski Z et al (2022) Reconnaissance analysis on buildings damaged during Durres earthquake Mw6.4, 26 November 2019, Albania: effects to non-structural elements. Bull Earthq Eng 20:795–817. https://doi.org/10.1007/s10518-021-01271-1

Srivastava HN, Verma M, Bansal BK, Sutar AK (2015) Discriminatory characteristics of seismic gaps in Himalaya. Geomatics Nat Hazards Risk 6(3):224–242

Subedi M, Sharma KCR, Misra K, J., KC A (2024) Reconnaissance of the effects of the M W5. 7 (M L6. 4) Jajarkot Nepal Earthquake of 3 November 2023, post-earthquake responses, and Associated lessons to be learned. Geosciences 14(1):20 https://doi.org/10.3390/geosciences14010020

Tamiminia H, Salehi B, Mahdianpari M, Quackenbush L, Adeli S, Brisco B (2020) Google Earth Engine for geo-big data applications: a meta-analysis and systematic review. ISPRS J Photogrammetry Remote Sens 164:152–170

Tobita T, Kiyota T, Torisu S, Cinicioglu O, Tonuk G, Milev N, Contreras J, Contreras O, Shiga M (2024) Geotechnical damage survey report on February 6, 2023 Turkey-Syria Earthquake, Turkey. Soils Found 64(3):101463. https://doi.org/10.1016/j.sandf.2024.101463

Upreti BN (1999) An overview of the stratigraphy and tectonics of the Nepal Himalaya. J Asian Earth Sci 17(5–6):577–606

USGS (2023) M5.7-44 km E of Dailekh, Nepal. United States Geological Survey: Reston, VA, USA

USGS (2024) United States Geological Survey: Reston, VA, USA. Data retrieved from: https://www.usgs.gov/fire-danger-forecast/weekly-ndvi and https://www.usgs.gov/landsat-missions/landsat-soil-adjusted-vegetation-index

Walker BB, Schuurman N, Swanlund D et al (2021) GIS-based multicriteria evaluation for earthquake response: a case study of expert opinion in Vancouver, Canada. Nat Hazards 105:2075–2091. https://doi.org/10.1007/s11069-020-04390-1

Ziotopoulou K, Cetin KO, Pelekis P et al (2022) Geotechnical reconnaissance findings of the October 30 2020, Mw7.0 Samos Island (Aegean Sea) earthquake. Bull Earthq Eng 20:7819–7852. https://doi.org/10.1007/s10518-022-01520-x

Authors and Affiliations

Rajan KC[1] · Richa Pokhrel[1] · Prabin Acharya[2] · Keshab Sharma[3] · Mandip Subedi[4] · Shikshita Bhandari[5] · Kabin Lamichhane[1]

✉ Keshab Sharma
ksharma@bgcengineering.ca

Rajan KC
rajankc.ioe@gmail.com

Richa Pokhrel
richapokhrel18@gmail.com

Prabin Acharya
pachary2@ualberta.ca

Mandip Subedi
mandip.subedi@gmail.com

Shikshita Bhandari
shikshitabhandari@stanford.edu

Kabin Lamichhane
kabin.762416@thc.tu.edu.np

[1] Geoinfra Research Institute, Lalitpur, Nepal

[2] Department of Civil and Environmental Engineering, University of Alberta, Edmonton, Canada

[3] BGC Engineering Inc, Fredericton, NB, Canada

[4] Universal Engineering and Science College, Lalitpur, Nepal

[5] Department of Earth System Science, Stanford University, Stanford, USA